4.1 Introduction

Efficient hydrogen generation by using solar light via water splitting is a demanding area of research for clean and sustainable energy generation [60]. Titanium dioxide (TiO_2) has been used for photocatalytic applications due to its high chemical stability, low toxicity, and its potential capability for the destruction of organic compounds in wastewater [60, 100, 101]. However, the efficiency of this wide bandgap (E_g~3.2 eV) TiO_2 is gravely limited for the utilization of visible light [102, 103]. Therefore, till date, several methods have been used to improve its absorption, including metal, nonmetal, and metallic ion doping that are capable to reduce its bandgap and enhanced the photocatalytic properties under visible light [104, 105]. Also, the deposition of novel metal nanoparticles (Ag [106], Au [107], Pd [19]) in combining with TiO_2 can improve the photo-electrocatalytic efficiency via hot-electron generation by surface plasmon resonance that effectively enhanced photocurrent generation [66, 85, 98, 108-110]. Besides that, an alternative way to enhance the absorption of TiO_2 is by heterojunction formation with lower bandgap metal sulfides (M_2S such as M = Ag, Cu) [73, 111, 112]. However, to date, photo-electrocatalytic efficiency of M_2S-TiO_2 heterojunction photoanode is not very efficient mainly due to the poor charge separation rate through the interface of heterojunction. Therefore, it is required to develop a technique for the creation of intimate contact of M_2S and TiO_2 to control, the band offset, which is the driving force at the interface of these two semiconductors for the interfacial charge transfer process [113, 114].

So far, a series of M_2S-TiO_2 heterojunctions, including CdS [115], Cu_2S [111], Ag_2S [73] MoS_2 [116] NPs have been widely studied, which are commonly deposited on top of

the TiO_2 surfaces. Among them, Cu_2S is considered an excellent candidate because of its ideal bandgap (1.2 eV) [117, 118], high absorption coefficient (>104 cm^{-1}), and good semiconducting nature [113, 117]. Instead of that, the performance of Cu_2S NPs for photoelectrochemical based H_2 generation is still very low which is due to the poor heterojunction formation between Cu_2S and TiO_2 with considerably high interface trap state [113, 119, 120]. Therefore, in our present study, a unique approach has been developed to grow electronically coupled Cu_2S NPs within titanium oxide (TiO_2) thin film and has been utilized for photocatalytic H_2 generation. This thin film growth consists of three successive steps, including sol-gel-derived ion-conducting thin film fabrication containing loosely bound light ion (Li^+) followed by ion-exchanged (with Cu^+) and subsequent sulfurization process. In this process, uniform and large-area Cu_2S-TiO_2 thin films are fabricated that contain Cu_2S NPs, ranging from 10 to 20 nm. The photo-electrocatalytic performance of Cu_2S-TiO_2 composite thin films was studied by photo-electrochemical water splitting experiment as discussed in subsequent sections. A charge transfer-enhancement synergistic mechanism has been discussed to explain the experimental results.

4.2 Results and Discussions

4.2.1 Structural and Surface morphology characterization

The crystal structure and phase confirmation of those thin films were analyzed by using a Rigaku X-ray diffractometer with Cu-Kα radiation (λ = 1.54 Å) in the 2θ range of 10^o – 90^o with a scan rate of 2°/minute. **Figures 4.1(a)** shows the x-ray diffraction (XRD) pattern of pure TiO_2 and $Li_4Ti_5O_{12}$ (LTO) thin film that has been deposited on FTO substrate by the dip-coating method. The diffraction peaks of LTO are located at 2θ ~ 18.5,

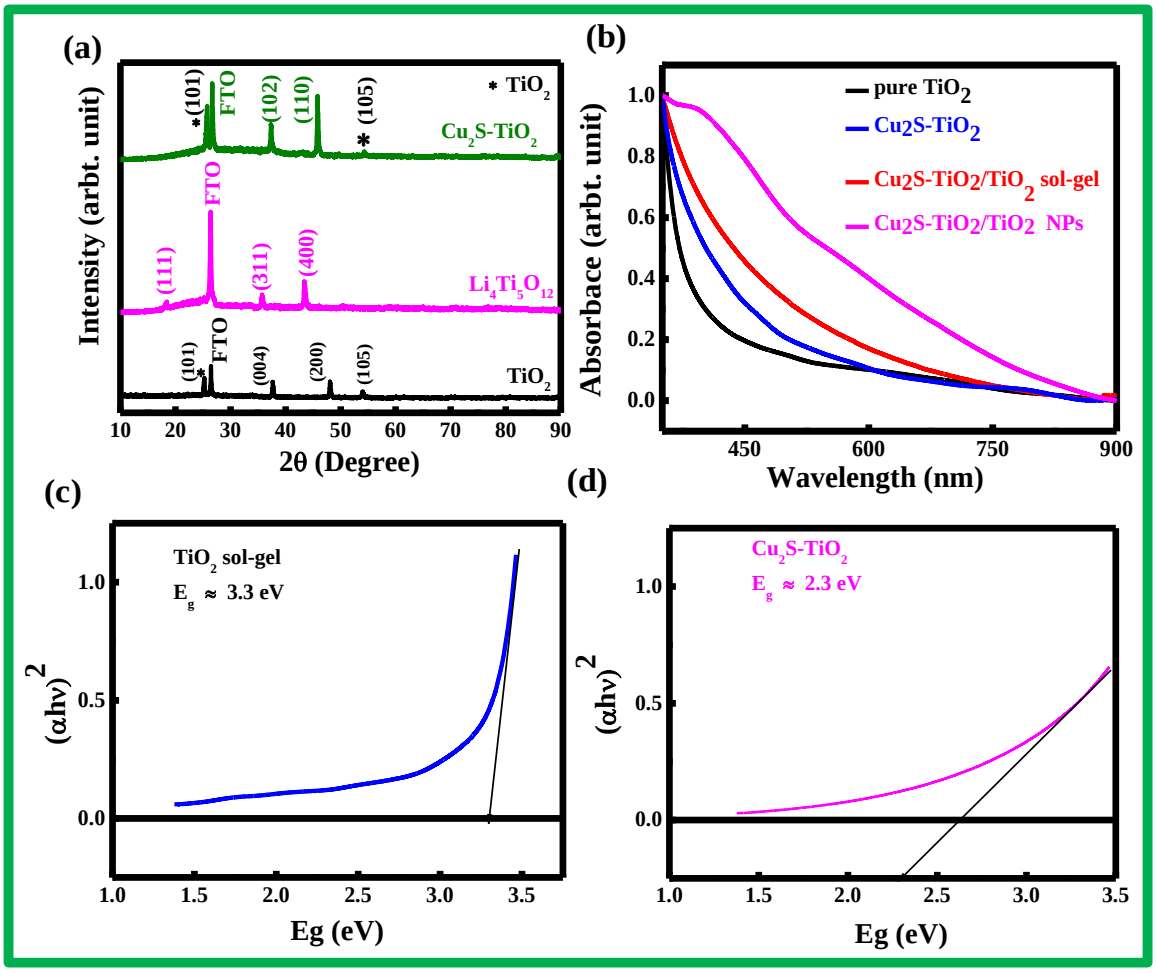

Figure 4.1*: (a) The XRD pattern of bare TiO_2, LTO and Cu_2S-TiO_2 (CSTO) thin films on the FTO substrate (b) Normalized UV-VIS absorption spectra of TiO_2 only and Cu_2S-TiO_2 coated with three different substrate including FTO, TS/FTO, and TN/FTO nanocomposite thin films (c-d) Taue plot from UV-VIS absorption spectra of (c)TiO_2 only (d)Cu_2S-TiO_2 coated thin films.*

35.6, 43.7, and the corresponding diffraction planes are (111), (311), (400). Those peak positions have been well-matched with JCPDS file no. 490207, indicates the cubic spinel structure of LTO with the space group of ($F\bar{3}dm$). The diffraction peaks of TiO_2 are identified at 2θ ~25.36°, 37.88°, 48.11°, 54.12° which are due to the diffraction plane of (101), (004), (200), (105) respectively (JCPDS No. 894921), indicates the tetragonal

structure with the space group of ($I4_1$). The diffraction peaks of Cu_2S-TiO_2 thin film that has been shown in **figure 4.1(a)** indicates the peak positions of Cu_2S-TiO_2 (green color) at

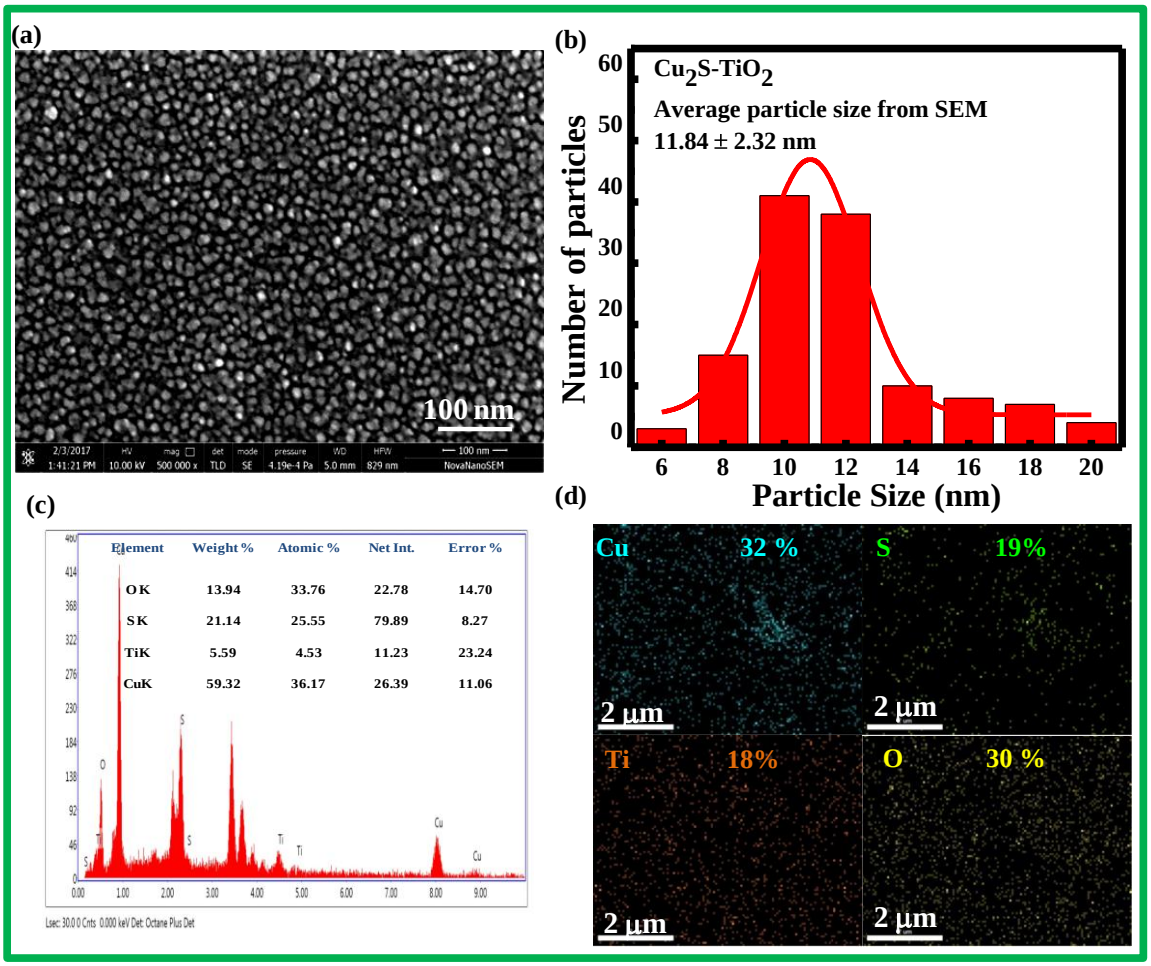

Figure 4.2 *The microstructure and surface morphology of the (a)* **Cu2S-TiO2 (dip coated) thin film** *on glass substrate (b) Particle size distribution of Ag-NP (c) Energy dispersive spectra of* **Cu2S-TiO2** *thin film, an elemental composition that obtained from EDS is shown in the inset. (d) EDS mapping of* **Cu2S-TiO2** *thin film (i) Cu(ii) for S, (iii) for Ti, and(iv) for O.*

2θ ~33.45°, 45.96° for Cu_2S, corresponding diffraction planes are (102), (110), well match with JCPDF number 892670. TiO_2 has three different crystallographic phases of (a) rutile (b) anatase and (c) brookite, and among this anatase is thermodynamically most stable phase [121]. This XRD study of Cu_2S-TiO_2 thin film has identified the formation of the anatase phase that has a peakposition at 2θ ~25.45° and 54. 25°[104, 121].

Figure 4.1(b) shows the normalized UV-VIS absorption spectra of pure TiO_2 and Cu_2S-TiO_2 thin with three different substrates, including FTO, FTO/TiO_2 (sol-gel), and FTO/TiO_2 NP film covering the range of 300-900 nm. Absorption spectra of TiO_2 thin film show stronger absorption in the UV region (300 nm) with a steadily lower absorption in higher wavelength of light, which is expected from wide bandgap TiO_2 (3.3 eV) thin film **(figure 4.1(c)**. On the other hand, in the case of Cu_2S-TiO_2 thin film, it shows significantly enhanced absorption in visible region due to the narrow bandgap nature of Cu_2S (1.2 eV) [118] nanocrystal **(figure 4.1(d)**.

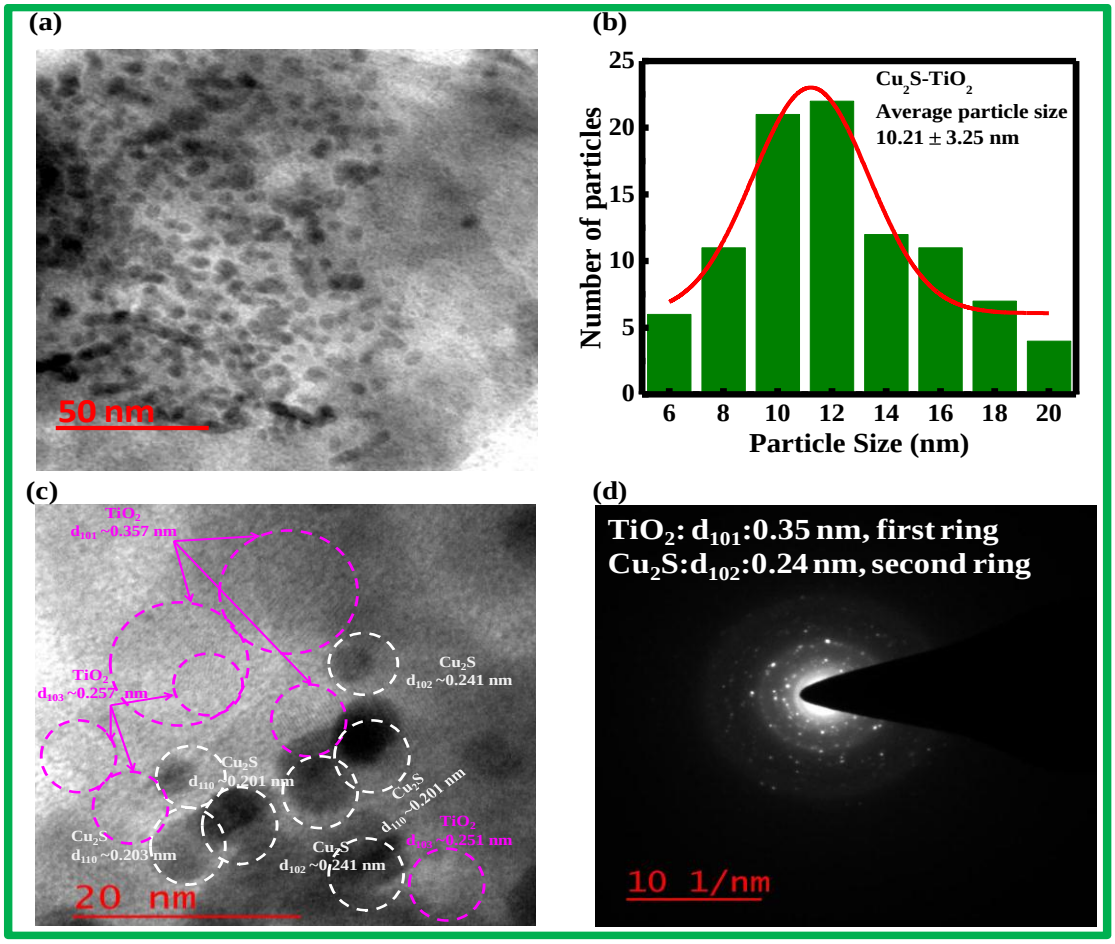

Figure 4.3 *(a) Transmission electron microscope image of Cu_2S NP-TiO_2 (b) size distribution of Cu_2S NP-TiO_2 (c) high resolution image of Cu_2S NP-TiO_2, white circle indicates the lattice d-fringe of Cu_2S and magenta circle for TiO_2 (d) selected area electron diffraction (SAED) pattern of Cu_2S NP-TiO_2.*

4.2.2 The surface morphology and microstructure characterization

The surface morphology and structural analysis of Cu_2S-TiO_2 thin film were investigated by high resolution scanning electron microscopy (HR-SEM) which is shown in **figure 4.2(a)**. These Cu_2S-TiO_2 thin film samples were prepared on the glass substrate as mention earlier. The SEM image of Cu_2S (NP)-TiO_2 shows the uniform particle distribution and with an average particle size of 11 nm. The size distribution has been shown in **figure 4.2(b)**. The content of the metallic element of the Cu_2S-TiO_2 sample was determined by an energy dispersive X-ray spectrometer (EDX) attached to the HR-SEM which is shown in **figure 4.2(c)**. The elemental mapping of Cu_2S-TiO_2 thin film is shown in **figure 4.2(d)**. These two pictures indicate the existence of Cu and Ti, S, and O elements inside thin film with a stoichiometric ratio.

The more detail of the structural analysis has been done by transmission electron microscopy (TEM) study, which is shown in **figure 4.3**. For sample preparation of this study, Cu_2S-TiO_2 thin film was scratched from the substrate and made a fine powder by using a grinding mortar that was dispersed in chloroform by keeping the solution under ultrasonic bath for 1 hour. **Figure 4.3(a)** demonstrated Cu_2S NPs formation within the TiO_2matrix, which is identified due to the higher contrast of Cu_2S than TiO_2. This picture also shows that the particle size is distributed mostly within the range of 7-21 nm with an average particle size of 10 nm. This distribution is very much similar to SEM analysis that shown in **figure 4.3(b)**. High-resolution TEM image **(Figure 4.3(c))** of Cu_2S (NPs)-TiO_2 show the lattice fringe formation of Cu_2S-NP and TiO_2 individually and their co-existence. The measured averaged d-spacing value of Cu_2S NPs and TiO_2 are 0.24 and 0.35nm respectively, that is corresponding to Cu_2S (102) and anatase TiO_2 (101) planes. These

planes are also identified with selected area diffraction pattern, which has been shown in **figure 4.3(d)** and the XRD analysis of Cu_2S-TiO_2 sample **(Figure-4.1(a))**.

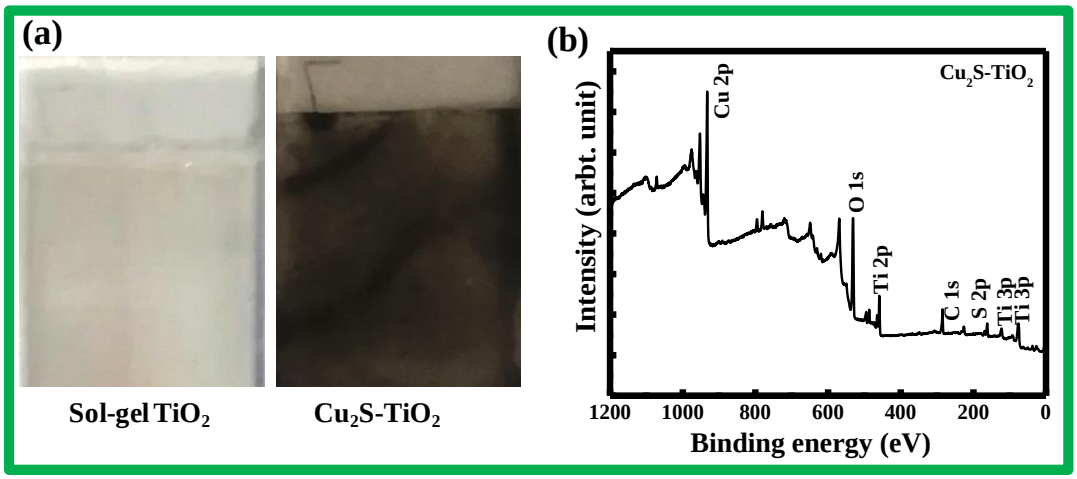

***Figure 4.4**: (a) The Image of the samples, bare TiO_2, and Cu_2S-TiO_2 (CSTO) thin films on the FTO substrate, (b) Survey scan of XPS for the Cu_2S-TiO_2 thin film.*

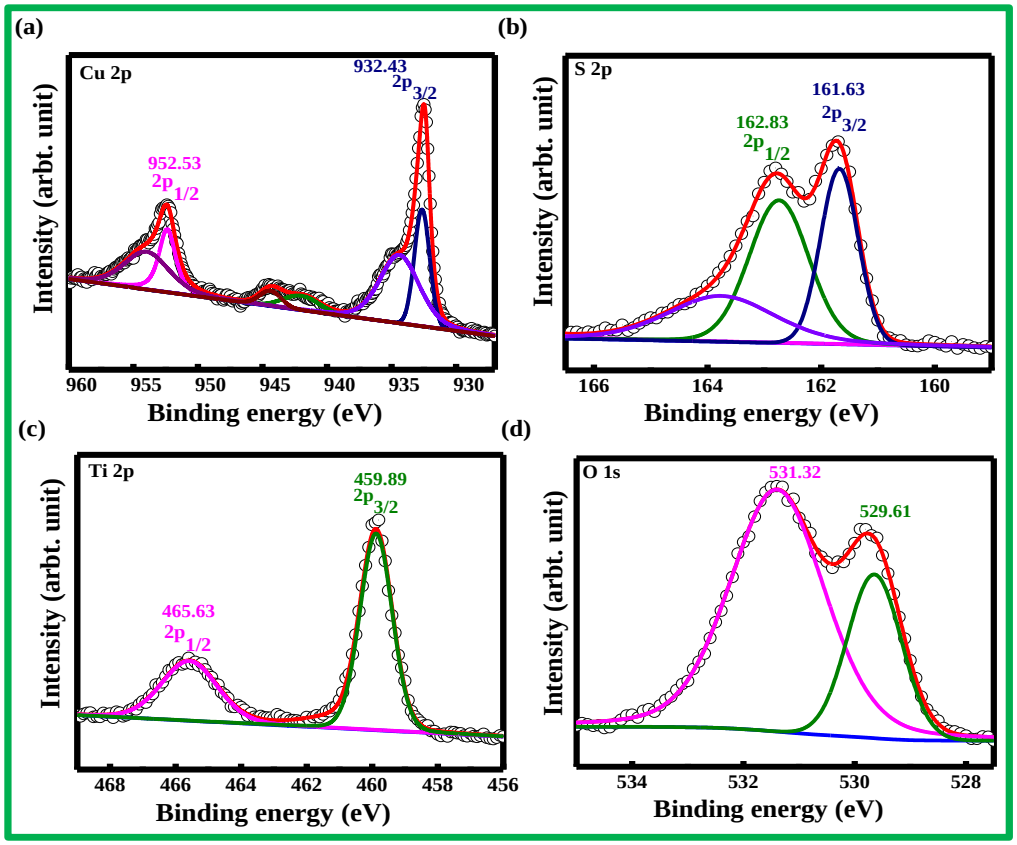

***Figure 4.5**:High-resolution XPS spectra of Cu_2S-TiO_2 sample (a) Cu 2p (b) S 2p (c) Ti 2p and (d) O 1s.*

4.2.3 X-ray photoemission spectroscopy (XPS)

The (XPS) study was conducted to investigate the chemical oxidation state of the elements presented in Cu_2S-TiO_2 nanocomposite thin film. The survey scan of XPS for the Cu_2S-TiO_2 thin film shown in **figure 4.4(b)** and deconvoluted XPS spectra of Cu 2p, S 2p, Ti 2p, and O 1s are shown in **figure 4.5(a-d)**, respectively. **Figure 4.5(a)** shows that the Cu 2p has two intense peaks at 952.53 and 930.43 eV which corresponds to the binding energy of Cu $2p_{3/2}$ and Cu $2p_{3/2,}$ respectively [122]. Similarly, two peaks of **figure 4.5(b)** appear for S 2p at 162.23 eV and 160.13 eV, which is characteristic for S^{2-}, which indicates that the formation of Cu_2S [122].

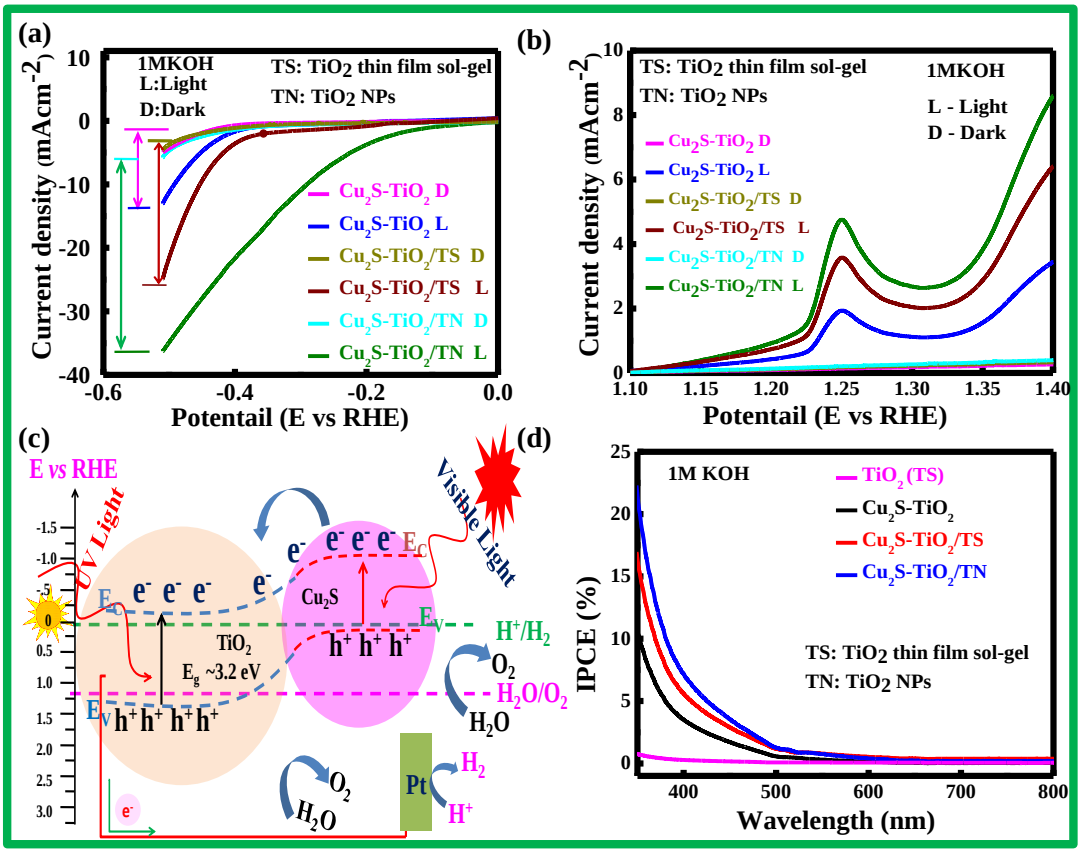

Figure 4.6 (a-b) *Current density vs. (V vs. RHE) potential of different Cu_2S-TiO_2 thin film under light and dark in 1 M KOH solution with three different substrates (a) for HER evolution, (b) for OER evolution (c) Schematic charge transfer process of Cu_2S-TiO_2 interface and H_2 evalution,(d) IPCE of bare TiO_2, Cu_2S-TiO_2 with three different substrates.*

Similarly, two peaks for Ti $2p_{1/2}$ and Ti $2p_{3/2}$ at 465.63 eV and 459.89 eV have been observed which are characteristic for Ti^{+4}, are shown in **figure 4.5(c)**. Besides those peaks, two more peaks are observed for O 1s at the binding energies of 531.32 eV, 529.61 eV, which correspond to O in TiO_2 and oxygen vacancies respectively[122], as shown in **figure 4.5(d)** and this indicates the formation of the and Ti-O-Ti bonding [123]. All these peak positions are well matched with earlier reported Cu_2S-TiO_2 systems [122, 124].Therefore, the XPS study of this sample gives another proof of the formation of Cu_2S-TiO_2.

4.2.4 Photoelectro-chemical H_2 generation study

The I-V curve of the Cu_2S-TiO_2 photoanode with three different substrates including, FTO, TiO_2 (sol-gel)/FTO, and TiO_2 NPs/FTO) in 1 M KOH solution under dark and light (100 mW/cm^2) conditions. As shown in **figure 4.6(a-b)**, there is around one order difference of current between light and dark conditions. The mechanism of the charge transfer process of the photoelectrochemical water splitting for the Cu_2S-TiO_2 system shown in **figure 4.6(a)**. Again photocurrent of Cu_2S-TiO_2 photoanode increases considerably in addition to the underlying TiO_2 layer in both cases H_2 evolution reaction (HER) shown in **figure 4.6(a)** and oxygen evolution reaction (OER) shown in **figure 4.6(b)**.The highest photocurrent was observed with Cu_2S-TiO_2 photoanode over TiO_2 NPs/FTO substrate with a current density of ~36 mA cm^{-2} at -0.5 V external bias for HER. To the best of our knowledge, this current density significantly higher with respect to earlier publications on the Cu_2S-TiO_2 system with similar geometries [96, 111, 124-126]. From this comparison, it's very clear that the charge transport rate through these electronically coupled *in-situ* grown Cu_2S-TiO_2 heterojunction is superior with respect to

the earlier reported. Again, this current density is 3000 times higher compared to TiO_2 only coated photoanode (0.012 $mAcm^{-2}$) under the same visible light illumination (**Figure 4.7(a)**). This enhancement of photocurrent density has been occurred due to the two main reasons. One of them is due to the higher absorption coefficient, i.e. larger amount of solar light absorption by low bandgap Cu_2S NPs [111, 122] that results a large enhancement of photogenerated electron-hole generation. Another reason is the higher charge transfer rate of the photogenerated electron from electronically coupled Cu_2S NPs to TiO_2, resulting in a significant reduction of the electron-hole recombination. This phenomenon has been schematically presented in **figure 4.6(c)**.This picture indicates that as soon visible light is illuminated on Cu_2S-TiO_2 photoanodes, major part of that spectrum is absorbed by lower bandgap Cu_2S NPs and generates electron-hole pair. This photogenerated electron of Cu_2S NP is then transferred to the CB of TiO_2. This charge transfer process of Cu_2S/TiO_2 heterojunction is energetically favorable because of the existence of CB of Cu_2S above that of TiO_2. Of course, a small fraction of the solar spectrum that lies in the UV region is absorbed by TiO_2 and generates electron-hole pair. The photogenerated electron of Cu_2S-TiO_2 thin film is then transferred from CB of TiO_2 to the FTO electrode. From there, photogenerated electron transports to the Pt cathode whereit produces H_2 gas. Similarly, photogenerated hole of TiO_2 is added with the photo generated hole of Cu_2S NP due to the existence of VB of Cu_2S NP above the VB of TiO_2. These photo generated holes of Cu_2S NP are then reacted with electrolyte solution, which produced OH and H^+ that has been described by equation (4.1-4.8). These h^+ ions then reach to Pt cathode through electrolyte where it accepts an electron to form H atom and subsequent H_2 molecules. As observed in our photo-electrochemical study, these charge transfer processes can be enhanced by an

additional TiO_2 thin film that results higher photocurrent generation with respect to Cu_2S-TiO_2 only photoanode. This is due to the larger area heterojunction formation between Cu_2S and TiO_2 due to an additional TiO_2 layer that helps higher rate charge transfer to the FTO electrode.

In electrolyte

$$H_2O \longrightarrow OH^- + H^+ \quad (4.1)$$

At anode

$$TiO_2 + hv\ (UV\ light) \longrightarrow CB_{TiO_2}(e^-) + VB_{TiO_2}(h^+) \quad (4.2)$$

$$Cu_2S + hv\ (visible\ light) \longrightarrow CB_{Cu_2S}(e^-) + VB_{Cu_2S}(h^+) \quad (4.3)$$

$$CB_{Cu_2S}(e^-) + TiO_2 \longrightarrow VB_{Cu_2S}(h^+) + CB_{TiO_2}(e^-) \quad (4.4)$$

$$CB_{Cu_2S}(e^-) + CB_{TiO_2}(e^-) \longrightarrow VB_{Cu_2S}(h^+, h^+) + CB_{TiO_2}(e^-, e^-) \quad (4.5)$$

$$VB_{Cu_2S}(h^+) + OH^- \longrightarrow OH + H^+ \quad (4.6)$$

$$4OH \longrightarrow 2H_2O + O_2 \quad (4.7)$$

At counter electrode

$$2H^+ + 2e^- \longrightarrow H_2 \quad (4.8)$$

4.2.5 IPCE Measurements

The rate of photocurrent generation in the different spectral ranges has been studied by measuring IPCE data of different photoanodes. A comparative study for IPCE data of bare TiO_2 (sol-gel) photoanode and Cu_2S-TiO_2photoanodes with three different substrates under -1.0 V external bias has been shown in **figure 4.6(d)**. IPCE spectrum of all Cu_2S-TiO_2 photoanode is very much similar, with a very strong photocurrent generation in the spectral region of 350-500 nm. In contrast to these data, TiO_2 (sol-gel) photoanode contribution a very week photocurrent that generated mostly bellow 400 nm, which is due to the wide bandgap nature of TiO_2. These features of IPCE data indicated that the major part of the photocurrent, which is associated withH_2 generation is originated from the Cu_2S

NPs. Again, comparative IPCE studies of different Cu_2S-TiO_2 photoanode shows that the highest value of IPCE has been achieved for the Cu_2S-TiO_2 /TiO_2 NPs/FTO sample with a value of ~ 22.56 % at 350 nm. This study implies that an additional TiO_2 layer always enhanced the charge transfer rate to the FTO electrode. Comparing TiO_2-NP and TiO_2 sol-gel thin film, the earlier one shows higher level photocurrent generation, is mostly due to the more crystalline and compact TiO_2 thin film that form relatively less internal trap states.

4.2.6 AC impedance study and Mott−Schottky (M-S) measurements

The electrochemical impedance spectroscopy (EIS) measurement for three different Cu_2S-TiO_2 photoanodes under dark and light are shown in **figure 4.7(c)**. As observed, there is a large difference of EIS data under dark and light for all these photoanodes, indicates a big variation of resistances because of white light illumination. The comparative EIS study shows that there are two semicircles for all Cu_2S-TiO_2 photoanodes. The semicircle diameter with Cu_2S-TiO_2/TiO_2 NP/FTO photoanode has the least value than two other photoanodes both under dark and light conditions. This result implies the resistance of Cu_2S-TiO_2/TiO_2 NPs/FTO photoanode is at least two others. Moreover, the smallest semicircles of EIS data of this photoanode also suggests that the charge transfer rate and photo generated electron-hole separation rate are higher than other samples [127].Inset of **figure 4.7(c)** shows the equivalent circuit of this electrochemical set-up that includes the solution resistance (R_S) in series with the parallel connection of interfacial charge-transfer resistance of the photoanode/electrolyte interface(R_1, R_2)and double-layer capacitance (C_1,C_2) associated with the charge transfer process. All EIS data are fitted according to this equivalent circuit. Summary of R_1 and R_2 for all three Cu_2S-TiO_2photoanode under dark and light conditions are given in **table 4.1**. Comparative EIS studies between pure TiO_2 and

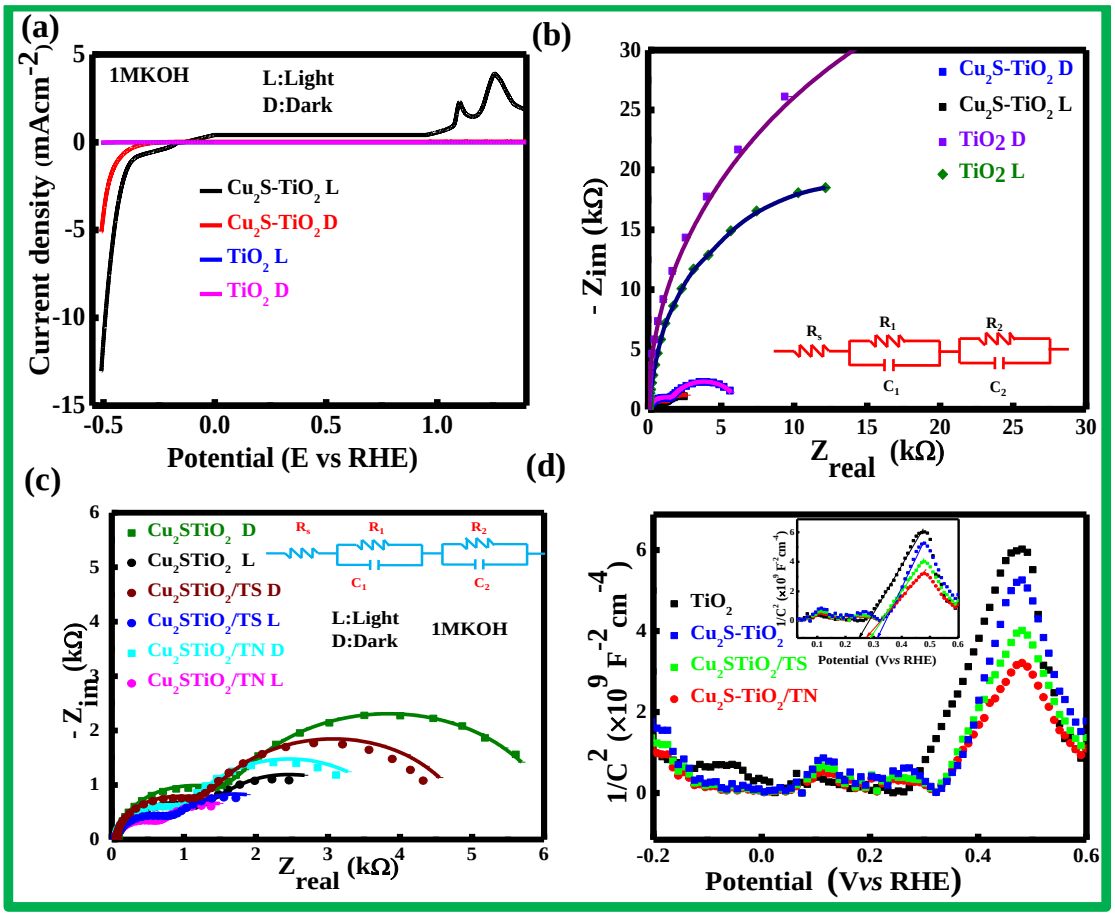

Figure 4.7*: The comparative study of (a) current density vs. (V vs. RHE) potential of bare TiO_2 and Cu_2S-TiO_2 thin film (b) EIS data of bare TiO_2 and Cu_2S-TiO_2 thin film (c) electrochemical impedance spectroscopy (EIS) measurement for three different Cu_2S-TiO_2photoanodes under light and dark conditions in 1 M KOH solution (d) The Mott−Schottky (M-S) plot for different photoanodes in 1 kHz operation under dark condition inset show the positive slop.*

Table 4.1: Summary of R_1 and R_2 for all three Cu_2S-TiO_2 photoanode under dark and light conditions.

Device structure	Rs (kΩ)		R_1 (kΩ)		R_2 (kΩ)	
	under dark	under light	under dark	under light	under dark	under light
Cu_2S-TiO_2	0.050	0.010	1.490	1.050	4.216	1.467
Cu_2S-TiO_2/TS	0.024	0.008	1.201	0.886	3.367	0.884
Cu_2S-TiO_2/TN	0.025	0.007	1.080	0.678	2.133	0.694

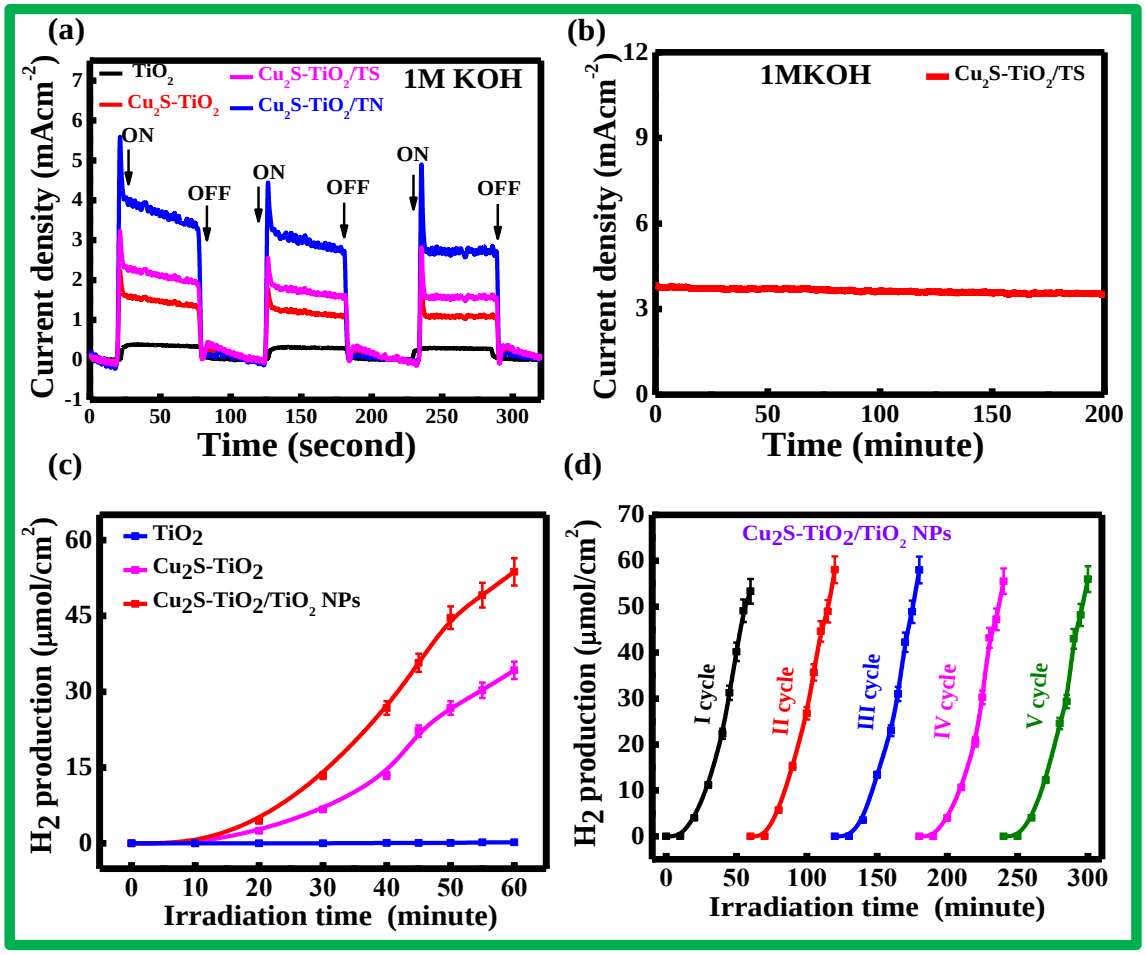

Figure 4.8: *(a)The time response of different photoanodes (b) the photostability of Cu_2S-TiO_2/TiO_2 sol-gel, (c) The volumetric hydrogen generation under one sun white light irradiation over the time for three different photoanodes. (d) For five successive cycle by Cu_2S-TiO_2/TiO_2 NPs photoaode.*

Cu_2S-TiO_2 photoanodes are shown in figure 4.7 (b) that shows the formation of Cu_2S-TiO_2 NPs inside TiO_2 thin film reduced the resistance of the photoanode both under dark and light conditions. The Mott−Schottky (M-S) measurements were carried out for a better understanding of the charge transport (electron) properties in photoanodes, which is shown in **figure 4.7(d)**. This experiment has been performed on different photoanodes coated with pure TiO_2 (sol-gel), Cu_2S-TiO_2, Cu_2S-TiO_2/TiO_2 sol-gel, and Cu_2S-TiO_2/TiO_2 NPs at an applied frequency of 1 kHz under dark conditions. The flat band potential (E_{FD}) of the

semiconductor-electrolyte interface and the surface charge density (N_D) values were calculated by using the Mott−Schottky equation [75].

$$\frac{1}{C^2} = \frac{2}{e\varepsilon_0\,\varepsilon_r N_D}\left(E_{app} - E_{FD} - \frac{kT}{e}\right) \quad (4.9)$$

Where C is the interfacial capacitance, E_{FD} is the flat band potential, k (1.3807×10^{-23}) is the Boltzmann constant; e is the electronic charge (1.6×10^{-19}coulomb), and T is the temperature of the system (~300K). The Mott−Schottky plot for different photoanodes shows a linear variation of $1/C^2$ with the applied potential. The M-S plot of all photoanodes shows a positive slope which indicated the n-type semiconductor interface nature of photoanodes. The flat potential (E_{FD}) of the photoanode was determined from the intersection of the slope with the x-axis of the plot. A positive shift of E_{FD} has been observed in all Cu_2S-TiO_2 photoanodes with respect to the reference TiO_2 photoanode, which implies a significant enhancement of charge transfer rate due to the formation of Cu_2S. The highest value of E_{FD} has been observed for Cu_2S-TiO_2/TiO_2 NPs coated photoanode, which implies the most efficient charge transfer rate among four different photoanodes. The surface charge densities (N_D) has been calculated by using the slop of M-S plot which is related by following equation [35, 75].

$$N_D = \frac{2}{e\varepsilon_0\,\varepsilon_r}\frac{dE}{d\left(\frac{1}{C^2}\right)} \quad (4.10)$$

It is observed that the extracted values of N_D are largely enhanced due to the Cu_2S-TiO_2 thin film formation with respect to TiO_2 (only) thin film. The highest value of N_D has been determined for Cu_2S-TiO_2/TiO_2 NPs thin film, which is responsible for the reduction in the ohmic resistance of the film that leads to improving the higher rate charge transfer from photoanode to the FTO electrode. The summary of E_{FD} and N_D values for all of these photoanodes are summarized in **table 4.2**.

Table 4.2 The summary of E_{FD}, N_A values for all of these photoanodes for n-type semiconductor.

Device structure	Slope from M-S curve at 1KHz	Negative Flat Band potential (+V)	N_A (cm^{-3})
Pure TiO_2	4.20×10^{9}	0.250	3.36×10^{18}
Cu_2S-TiO_2	3.24×10^{9}	0.321	4.35×10^{18}
Cu_2S-TiO_2/TS	2.73×10^{9}	0.271	5.17×10^{18}
Cu_2S-TiO_2/TN	2.18×10^{9}	0.292	6.47×10^{18}

4.2.7 Volumetric hydrogen generation rate and time response measurement

Time response of different photoanode under dark and light (100 mW/cm^2) with -0.5 V external bias has been shown in figure 4.8(a) for Cu_2S-TiO_2 that indicates that the photoresponse is repeatable. Rise time and fall time of Cu_2S-TiO_2/TiO_2(NP)/FTO are 2.10 S and 2.61 S, respectively which implies faster response of these photoanodes. Summary of rising and fall time of all samples are shown in table-4.3. The stability of Cu_2S-TiO_2 photoanode with TiO_2-NP underlying thin film was carried out in 1 M KOH for around 200 minutes under white light illumination.

Table 4.3 Summary of rise time and fall time of all samples.

Device structure	Raising time (Second)	Falling time (Second)
Pure TiO_2	3.82	6.85
Cu_2S-TiO_2	3.01	2.85
Cu_2S-TiO_2/TS	2.41	2.55
Cu_2S-TiO_2/TN	2.10	2.61

This data shows an initial growth of photocurrent which becomes stable over time, which indicates the good stability of this Cu_2S-TiO_2 thin film as shown in figure 4.8(b).

The hydrogen generation rate has been studied by continuous irradiation of white light of intensity 'one sun' and by collecting generated hydrogen over the time. This experiment has been performed with two different photoanodes of Cu_2S-TiO_2 thin film. One of them is with the TiO_2 (NPs) layer and the other one is without TiO_2layer. In addition, the TiO_2 (sol-gel) photoanode has been tested for references. As it has shown in **figure 4.8(c)**, the higher rate of H_2 has been generated by Cu_2S-TiO_2/TiO_2 NP/FTO photoanode with a production rate ~ 55 μmol/cm^2 which is almost ~1.2 times higher than Cu_2S-TiO_2/FTO photoanode. This H_2 generation experiment has been performed in five successive cycles with Cu_2S-TiO_2/TiO_2NP/FTO photoanodewhich is shown in **figure 4.8(d)**. As observed, this production rate is very much similar in all five different cycles.

4.3 Conclusions

In summary, large area electronically coupled Cu_2S (NP)–TiO_2 heterojunction thin film has been fabricated in a simple solution-based technique. This growth technique requires three successive steps that include the fabrication of $Li_4Ti_5O_{12}$ ceramic thin film by sol-gel technique followed by an ion-exchange process that replaces Li^+ by Cu^+ to form $Cu_4Ti_5O_{12}$ thin film. Finally, $Cu_4Ti_5O_{12}$ thin-film converted to Cu_2S-TiO_2 due to the chemical conversion of Cu^+ to Cu_2S. Such kind of *in situ* growth of Cu_2S NP inside TiO_2 allows forming a larger interface area of Cu_2S/TiO_2 composite with lesser interface trap states. The formation of Cu_2S-TiO_2 was confirmed by SEM, XRD, XPS and UV-VIS absorption study. Photoelectrochemical measurement was carried out of this Cu_2S-TiO_2 thin film photoanodes to identify its applicability for H_2 generation. For this study, Cu_2S-TiO_2 thin

films are grown on three different substrates including FTO, TiO_2 (sol-gel)/FTO and TiO_2 NP/FTO coated glass and the comparative photo-electrocatalytic measurement of these photoanodes showed that the sample on TiO_2 NP/FTO substrate generate the highest photocurrent of density 36 mA cm^{-2} in 1M KOH solution under 0.5 V external bias which is ~3600 times higher than TiO_2 (only) photoanode. Volumetric measurement shows that this H_2 generation rate is ~ 55 μmol/cm^2/hour. This photocurrent density and H_2 generation rate is significantly higher than earlier reported Cu_2S/TiO_2 system. Moreover, this photocurrent shows good stability that has been tested for more than 1.5 hours. In futuristic, the present process can be extended for the fabrication of other metal chalcogenides-metal oxide composite systems for different energy harvesting applications.